GSA DATA REPOSITORY 2015130

Supplementary Figures & Captions (DR1–DR7)

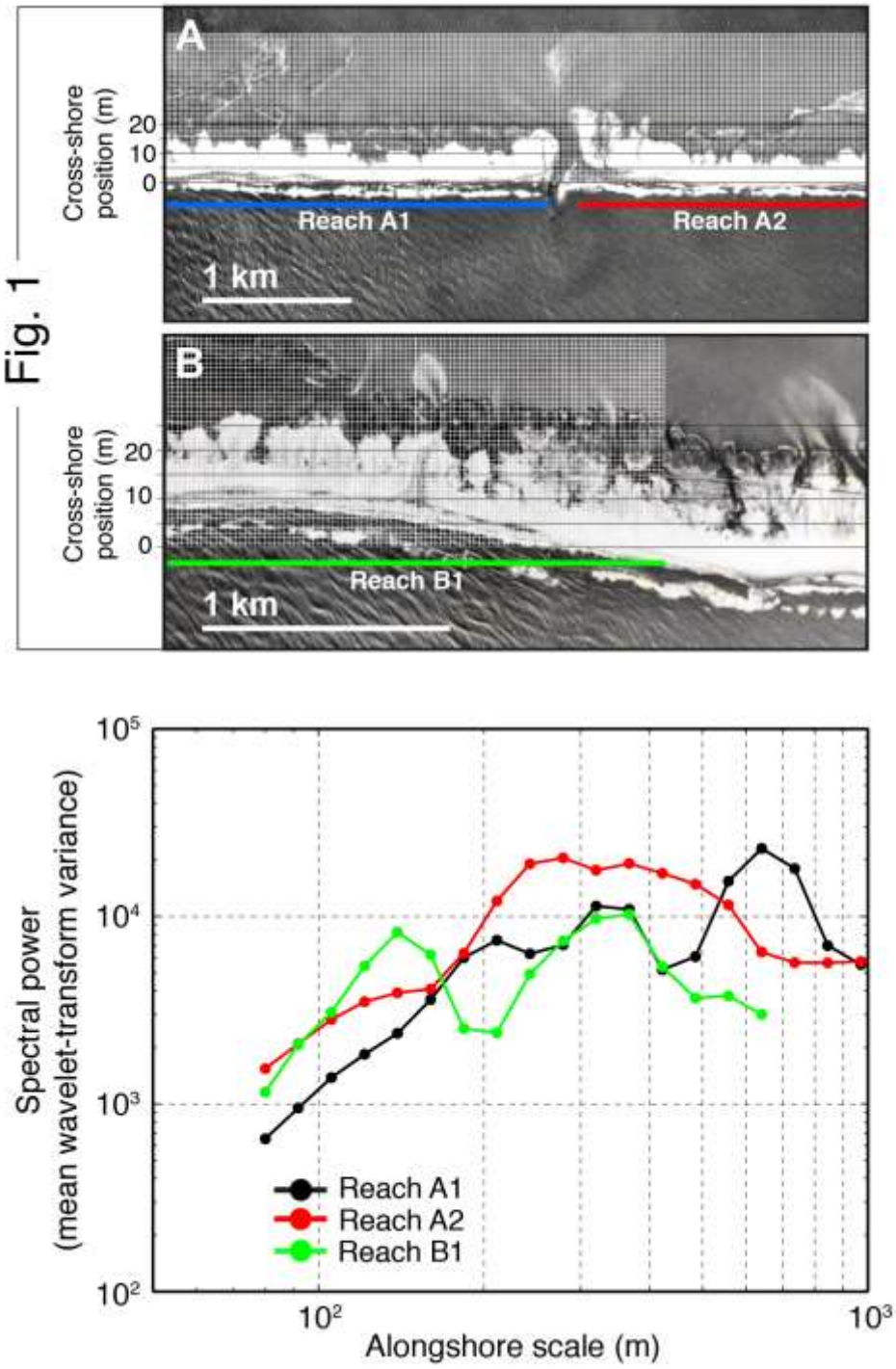

Figure DR1. To calculate the power spectra of the washover shown in Fig. 1, we superimposed square-lattice grids scaled to both photos, respectively, such that each grid square = ~20 m. We did not measure across the inlet evident in Fig. 1A.

Likewise, we measured only the first two-thirds of the barrier in Fig. 1B, up to where the washover planform becomes indistinct. Wavelet analysis of the resulting back-barrier shorelines (detrended) returns a dominant alongshore wavelength for Reach A1 ~600 m, a secondary peak ~350 m, and a tertiary saddle ~200 m. For Reach A2, a dominant wavelength is less pronounced (in agreement with the photograph), with roughly equivalent power across ~250–450 m wavelengths. Reach B1 appears bimodal, with a peak ~150 m and another ~300–350 m, consistent with where adjacent smaller-scale lobes have begun to merge.

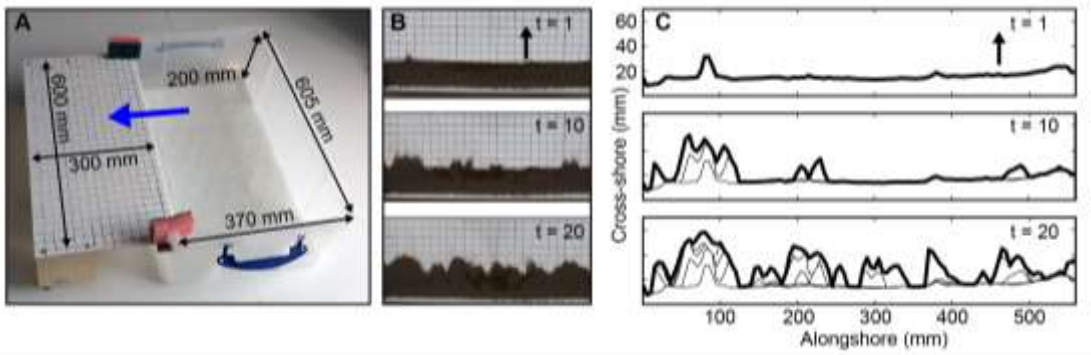

Figure DR2. (A) "Tub flume" apparatus used for the physical experiment. Blue arrow indicates flow direction. **(B)** Photo sequence showing plan-view changes in the experimental barrier during an experimental trial. **(C)** Superimposed, digitized back-barrier planforms extracted from orthorectified versions of the raw photos in B. Bold line marks back-barrier planform at time step shown. Black arrows in B and C indicate flow direction.

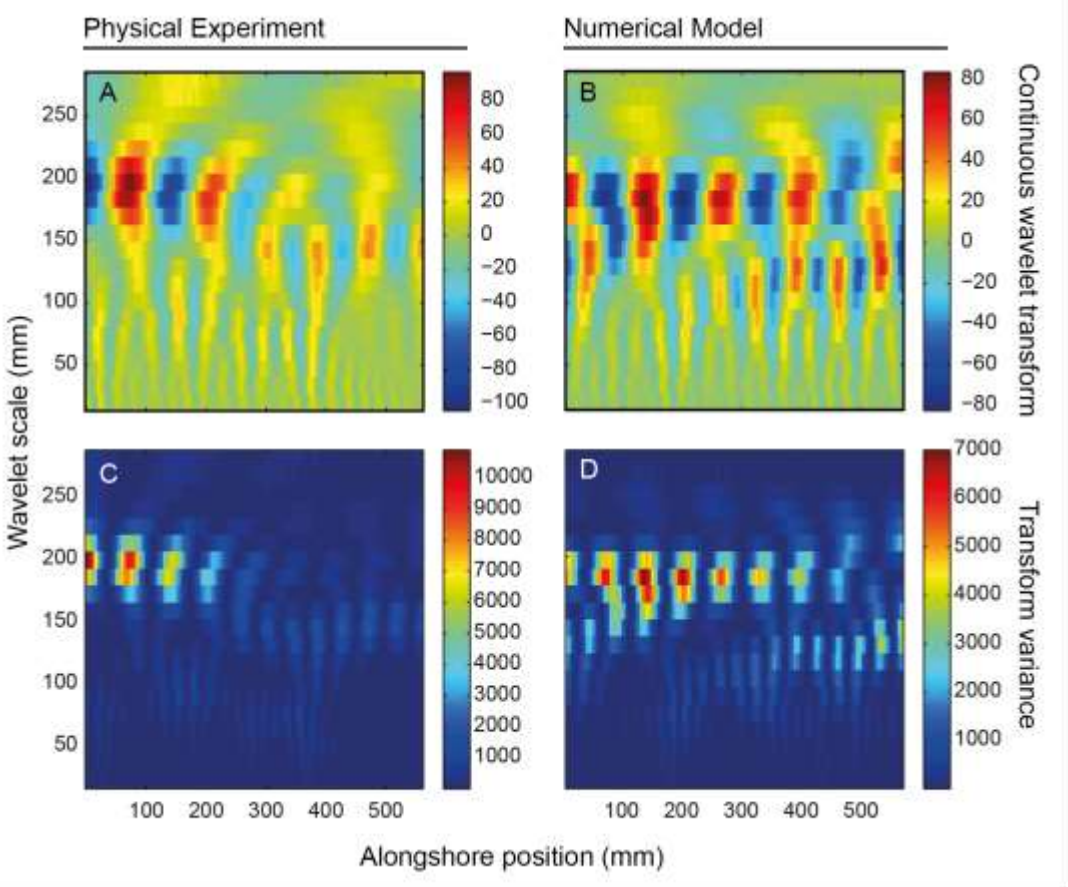

Figure DR3. A wavelet can walk along the signal in discrete steps, like a caliper, or slide continuously between consecutive points. We use the latter, called a continuous wavelet transform. Despite its sampling redundancy, a continuous transform can reveal spatial heterogeneities in the data in greater detail. Squaring the scaled wavelet transform yields a measure of signal variance. Calculating the mean variance at each scale produces a power spectrum much like a Fourier analysis. Using both the averaged power spectrum (Fig. 3) and the full wavelet transform (above) allows both a coarse summary and detailed quantitative description of patterns, often spatially localized, embedded in the data series. In this analysis we apply a Morlet wavelet,

$$\psi(f(x)) = \left(e^{-(f(x))^2/2}\right)\cos(5f(x))$$

a common waveform whose shape is conducive to resolving mesoscale features in a data series, where ψ is the wavelet transform and $f(x)$ is back-barrier shoreline

position (detrended). To minimize edge effects at the beginning and end of the original signal, we reflect the signal several times, convolve the extended signal, and then use an interior multiple of the transform. As a further precaution against edge effects, we also only consider spatial scales smaller than half the length of the data series. This figure shows continuous wavelet transforms for **(A)** the experimental and **(B)** numerical back-barrier planforms shown in Fig. 2E and Fig. 2J, respectively. Panels **(C)** and **(D)** show transform variance (the squares of the values plotted in A and B). Mean transform variance calculated at each wavelet scale yields the power spectra shown in Figs. 3E and 3J.

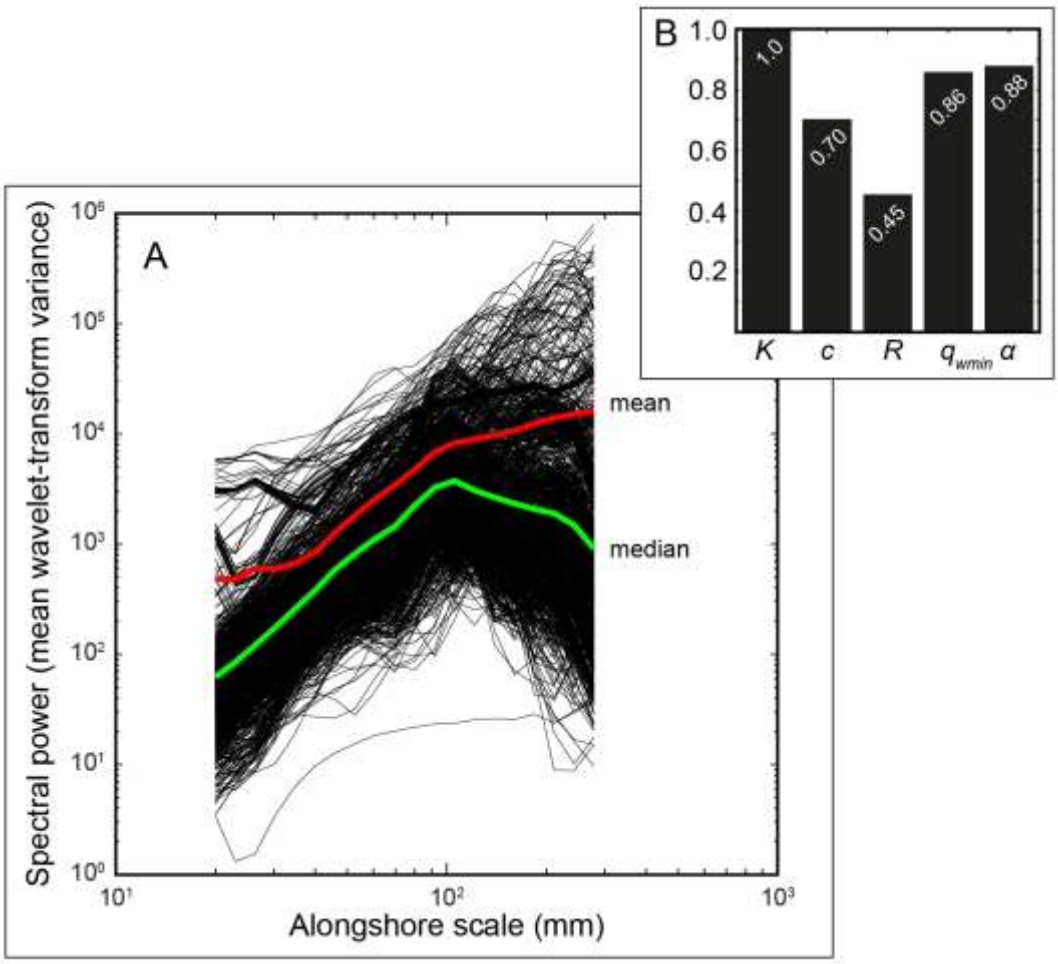

Figure DR4. (A) Power spectra at time step t = 25 for 9600 combinations of model parameters tested over the following intervals: diffusivity, K = 0:0.1:0.9; sediment-entrainment proportion, c = 0.1:0.1:0.4; radius of influence, R = 10:10:50; minimum water depth, q_{wmin} = 0:0.01:0.05; and topographic contour α = 0.01:0.01:0.08. The same stochastic sequences were used for each model run. Incision-depth proportion (b = 0.1) and transmissivity (T = 1 L T^{-1}) were held constant throughout. The ensemble mean and median spectra are plotted in red and green, respectively. The ensemble median spectrum (green) captures a dominant wavelength ~100 mm. **(B)** Normalized standard deviation in the power spectra resulting from varying each parameter in turn.

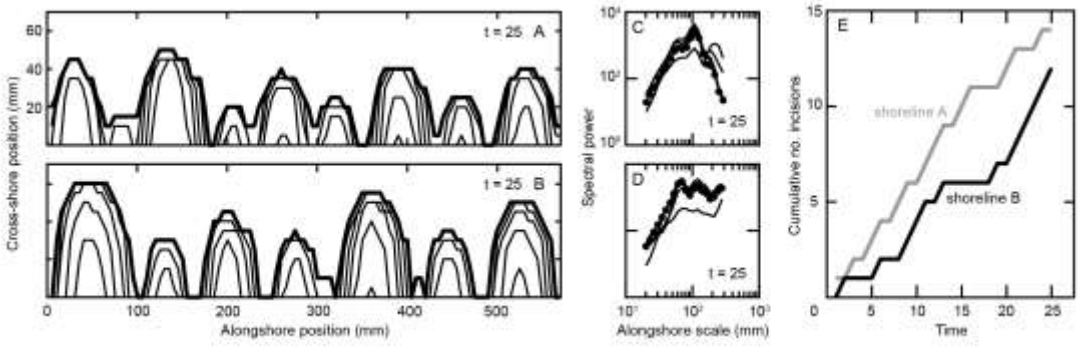

Figure DR5. Relative timing of washover emplacement during a storm event can affect the spectral signature of the back-barrier planform. Although the same parameter settings (see Fig. 2) were used to generate the planforms in **(A)** (same as Panel J in Fig. 2) and **(B)**, the randomized sequence in which new washover lobes were initiated differed between the two trials, resulting in unimodal **(C)** and bimodal **(D)** power spectra, respectively. The cumulative number of incisions over time in sequences A and B are shown in **(E)**. Fewer early-stage washover lobes may foster spectrum modes > 1, while a more continuous emplacement regime results in a strongly unimodal spectrum.

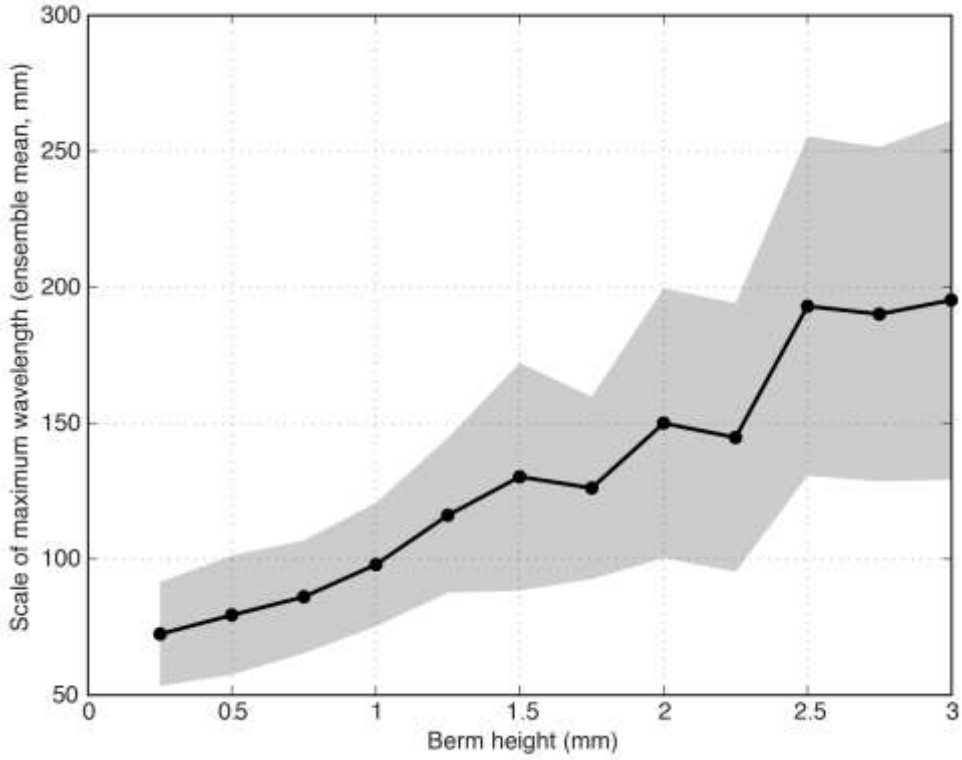

Figure DR6. Holding other dimensions in the numerical model held constant, changing barrier (berm) height exerts a strong, consistent control on dominant washover wavelength. This figure shows the mean scale of maximum wavelength (with gray envelope denoting ± 1SD around the mean) increasing with barrier height (Z_b). For a given height, the mean maximum wavelength is calculated from an ensemble of 30 trials with the same parameter settings but different stochastic sequences. Here, $I = J = 140$ (~5 mm cells), $K = 0.3$, $c = 0.25$; $R = 20$; $q_{wmin} = 0.02$; $\alpha = 0.02$ mm, $b = 0.2$, $T = 1$.

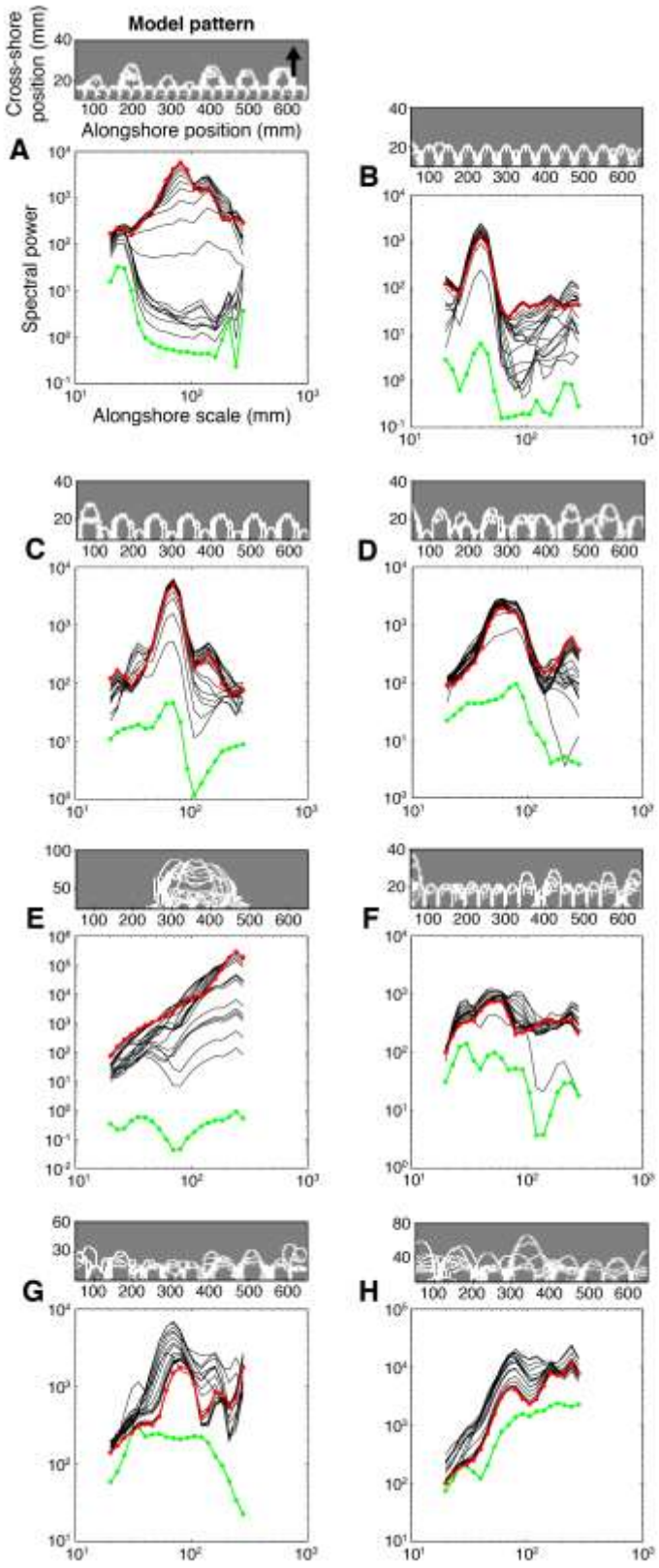

Figure DR7. This figure illustrates further exploration of self-organized washover behavior in the numerical model. Gray boxes showing back-barrier shorelines (white), where flow direction is bottom to top (black arrow), correspond to power spectra

immediately below, where the spectrum at $t = 1$ is in green and the final spectrum at $t = 30$ is in red (finer lines represent spectra at intermediate time steps). For the results shown, parameter settings are: $I = J = 140$ (~5 mm cells), $K = 0.3$, $c = 0.25$; $R = 20$; $q_{wmin} = 0.02$; $\alpha = 0.02$ mm, $b = 0.2$, $T = 1$, $Z_b = 1$. The same stochastic sequence is used for all trials. **(A)** The barrier is perturbed with an initial-condition ($t = 0$) "template" of equidistant incisions of equal depth at a spacing of 6 cells (~30 mm). In this case, the 30 mm template controls washover spacing for nearly half the trial, but the dense spacing breaks down when subtle differences in the alongshore hydraulic gradient begin to trigger new incisions, destabilizing the template-driven pattern and creating a new dominant wavelength (~70 mm). **(B)** The initial-condition ($t = 0$) template of equidistant, equal-depth incisions is set to 10 cell (~50 mm) and **(C)** 17 cell (~85 mm) spacing; in each case the template persists as the dominant washover wavelength. **(D)** When the barrier at $t = 0$ is perturbed at 15 random locations alongshore with incisions of equal depth, the barrier still adjusts to a dominant wavelength. **(E)** If initially perturbed at $t = 0$ with a single, large incision (8 cells wide to 80% the height of the barrier), the barrier demonstrates a runaway positive feedback: the initial throat is so large that no other incisions can compete for flow, and a single washover lobe dominates the back-barrier. **(F)** The barrier at $t = 0$ is perturbed every 7 cells alongshore (~35 mm) with incisions of random depths between 0–60% of the barrier height, again finding a final spectrum that differs from the initial condition. **(G)** and **(H)** show back-barrier patterns that evolve under two different stochastic sequences, respectively, for which the initial barrier is perturbed at 20 random locations alongshore with incisions of random depths between 0–60% of the barrier height.